Oct 17th, 12:00 AM

Compression Tests of Cold-reduced High Strength Steel Stub Columns

Demao Yang

Gregory J. Hancock

Sixteenth International Specialty Conference on Cold-Formed Steel Structures
Orlando, Florida USA, October 17-18, 2002

Compression Tests of Cold-Reduced High Strength Steel Stub Columns

Demao Yang[1] and Gregory J Hancock[2]

ABSTRACT

This paper describes a series of compression tests performed on stub columns fabricated from cold-formed high strength steel plates with nominal yield stress of 550 MPa. (80 ksi) The steel is classified as G550 to Australia Standard AS1397. The test results presented in this paper are the first stage of an Australian Research Council research project entitled "Compression Stability of High Strength Steel Sections with Low Strain-Hardening". The tests include lipped-square and hexagonal sections, including 94 box-shaped fix-ended stub columns. The purpose of these tests was to determine the influence of low strain hardening of G550 steel on the compressive section capacities of the column members. The results of the successful stub column tests have been compared with the design procedures in the Australian/New Zealand Standard for Cold-Formed Steel Structures and recent (1999) Amendments to the American Iron and Steel Institute Specification. As expected, the greatest effect of low strain hardening was for the stockier sections where material properties play an important role. For the more slender sections where elastic local buckling and post-local buckling are more important, the effect of low strain hardening does not appear to be as significant. This is contrary to recent design proposals in the USA where it was proposed that the more slender sections would be more greatly influenced by low strain hardening. A simple proposal for improved design capacity is given in the paper.

INTRODUCTION

The use of high strength steels with yield stress values up to 550 MPa (80 ksi) is increasing rapidly, particularly for steel framed houses with sections as thin as 0.42 mm (0.017 in.). Steels with high yield stress usually have little or no strain hardening in the stress-strain curve, and low ductility unlike conventional structural steel that is highly ductile and strain harden as shown in Yang and Hancock (2002). Strain hardening is important in the stability of thin-walled sections and so the high strength steels are likely to have their stability significantly affected by the lack of strain hardening.

1) Ph.D. candidate, Department of Civil Engineering, University of Sydney, N.S.W., Australia, 2006.
2) BHP Steel Professor of Steel Structures, Department of Civil Engineering, University of Sydney, N.S.W., Australia, 2006.

For high strength steel sections made from thin galvanized cold-reduced steel to Australian Standard AS 1397-1993, no specific investigation has been performed. Mainly due to lack of knowledge on their structural behaviour, the 1996 Australia/New Zealand Standard AS/NZS 4600 for Cold-Formed Steel Structures and the 1996 American Iron and Steel Institute (AISI) Specification for Cold-Formed Structural Members have limited the design stress for high strength steels to 75 percent of their yield stress or tensile strength as applicable. The AISI Specification has recently been revised in Supplement No.1 (1999) to allow values higher than 75 percent for multiple web configurations, the value depending mainly on plate slender.

A research project on these steels in tension, which was carried out by Rogers and Hancock (1996), has shown that they have substantially reduced ductility but this may not affect the net section strength of perforated sections. Steels of this type are similar to Structural Grade 80 steels in the USA according to the ASTM A653 (1997) Standard. A research project led by Professor W-W Yu at the University of Missouri-Rolla to investigate the strength of these ASTM steels when formed into decking sections and subject to bending has demonstrated that their local and post-local buckling capacities may be significantly influenced by the lack of strain hardening. In particular, the ultimate moments of panels with slender sections (b/t>100) were lower than the design moments calculated based on a conventional effective section model. However, no significant definitive testing has been performed for sections composed of AS 1397 steel in compression. The AS 1397 steel may be zinc-coated or aluminium-zinc coated. Those studied in this report were aluminium-zinc coated similar to ASTM A792 (1994).

The aim of this paper is to present the test results of the stub columns. The tests were performed on box (B), lipped-box (LB) and hexagonal (HB) shaped specimens of three different cross-sections fabricated from G550 steel sheets with 0.60 mm (0.024 in.) and 0.42 mm (0.017 in.) thickness. The specimens included stub columns and long columns. The stub columns were tested between fixed ends and the long columns were tested between pinned ends.

TEST SPECIMENS

General

The tests were performed on closed sections brake pressed from aluminium/zinc-coated Grade G550 structural steel sheet to AS1397. The sections tested are shown in Fig. 1 & 3. Epoxy was used to close the B & LB-sections and a Teflon/Steel Support was used to close the HB-sections. Bolts & clamps were also used on the B & LB-sections as discussed in Yang and Hancock (2002). The sections were fabricated from 0.42 mm (0.017 in.) and 0.60 mm (0.024 in.) steel sheets. The widths of the B-sections ranged from 20 mm (0.79 in.) to 100 mm (3.94 in.) for the 0.60 mm (0.024 in.) sheet steel and 14 mm (0.55 in.) to 70 mm (2.76 in.) for the 0.42 mm (0.017 in.) sheet steel. The flats of the HB-sections ranged from 20 mm (0.79 in.) to 100 mm (3.94 in.) and the thickness was 0.60 mm (0.024 in.). The holes/clamping configurations are shown in Fig. 1 & 3. The dimensions of the specimens are given in Appendix-1, for the nomenclature shown in Fig. 2. Further details are given in Yang and Hancock (2002).

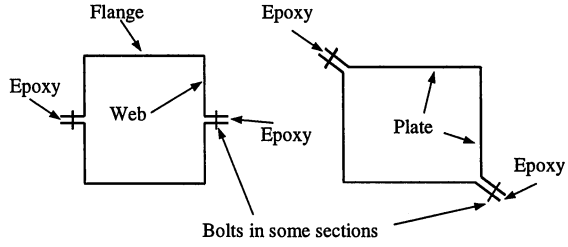

(a) Lipped-Box Section (LB) **(b) Box Section (B)**

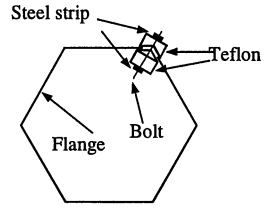

(c) Hexagonal Section (HB)

Fig.1 Test Sections

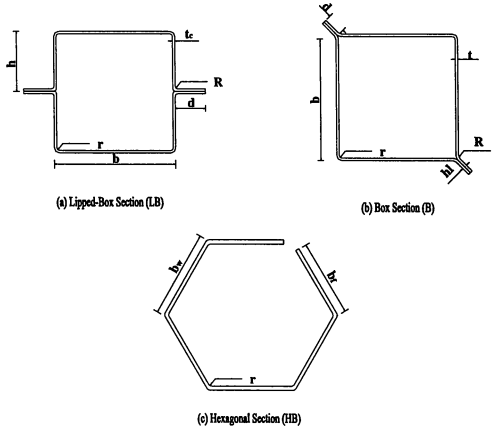

Fig.2 Cross-Section Dimension Nomenclature

For the B-sections, tests were performed on 0.60 mm (0.024 in.) thickness material and 0.42 mm (0.017 in.) thickness material. All sections had the same size lips. For the LB-sections, tests were performed on both 0.42 mm (0.017 in.) and 0.60 mm (0.024 in.) thickness material.

The lips of the LB-sections in 0.42 mm (0.017 in.) thickness were the same for all series. However, for the 0.60 mm (0.024 in.) thickness LB-sections, the lips were different from section size to size for the two series. The material used for the LB-sections had different yield stress values. For the HB-sections, tests were only performed on 0.60 mm (0.024 in.) thickness material. Two slotted pieces of Teflon and two long steel strips were used to join the two edges of the HB-sections together. The objective of the Teflon was to connect the longitudinal free edges without resisting axial compressive load. Further details are given in Yang and Hancock (2002).

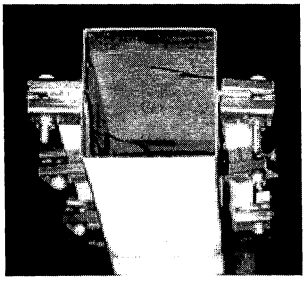

(a) Lipped-Box Section (LB) with Clamps

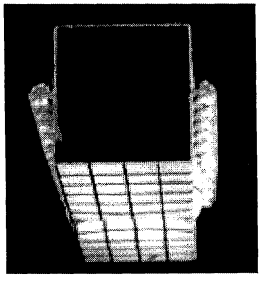

(b) Lipped-Box Section (LB) with Bolts

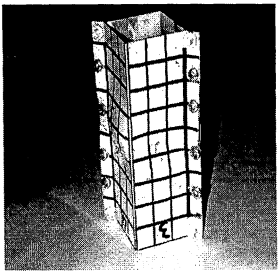

(c) Box Section (B) with Bolts

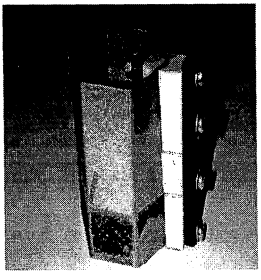

(d) Hexagonal Section (HB) with Teflon Support

Fig.3 Bolting & Clamping Configurations of Test Specimens

Labelling

The B & LB-sections were divided into two different series for 0.60 mm (0.024 in.) sheet steel and three different series for 0.42 mm (0.017 in.) sheet steel. The HB-sections had one series. The test specimens were labelled such that the thickness of steel sheet, type of section, nominal width of specimen and specimen number were expressed by the label.
For example, the label "060LB40ra" defines the following specimen:

- The first three numbers indicate that the specimen is fabricated from 0.60 mm (0.024 in.) steel sheet.
- The fourth and fifth letters (LB) indicate that the specimen is a lipped box (alternatives B for box and HB for hexagon).
- The "40" indicates that the nominal width of specimen is 40 mm (1.57 in.) (flat width for a hexagon).
- The "r" indicates that the specimen is a repeat test.
- The last letter "a" indicates that the specimen was the first tested (alternatives b, c).

Geometric Imperfection Measurements

The geometric imperfections were measured for the test specimens. All of the profiles of measured initial imperfections for the sections are given in Yang and Hancock (2002). Typical maximum average out-of-flatness values are 0.3 mm (0.012 in.).

MATERIAL PROPERTIES

Coupon Test specimens and procedures

The material properties of each series of specimens were determined by tensile coupon tests. Two longitudinal coupons were tested for each series of specimens. The coupon dimensions conformed to AS1391-1991 (Standards Australia, 1991) for the tensile testing of metals. In order to ensure that fracture occurred within the middle portion of the constant gauge length, the test coupons were dimensioned with a more gradual change in cross-section from the constant gauge width to the grip. Specimens were fabricated with larger radii (i.e. 55 mm (2.17 in.)), which required a shortening of the constant gauge length (Rogers and Hancock, 1996). The tensile coupons were 12.5 mm (0.49 in.) wide with gauge length 50 mm (1.97 in.).

The longitudinal coupons were tested according to AS1391 in the Sintech/MTS 300 kN (67 kips) testing machine. The coupons were tested with the aluminium/zinc coating removed. In the tests the longitudinal strains were measured using two strain gauges for every coupon, which were attached at the centre of each face. A SPECTRA data acquisition system was used to record the load and readings of strain during the test.

Coupon test results

The stress-strain curves were obtained from the coupon tests using strain for 0.42 mm (0.017 in.) and 0.60 mm (0.024 in.) material respectively. The yield stress f_y was obtained using the nominal 0.2% proof stress. The stress was the measured load divided by the initial cross-section area of the coupon and the strain is the average of the two strain gauge readings. The measured 0.2% proof stress of the steel ranged from 634 MPa (92 ksi) to 711 MPa (103 ksi). Young's modulus of elasticity (E) was also calculated from the elastic part of the stress-strain curves using Mathcad. The calculated mean values of Young's modulus of elasticity were 2.20×10^5 MPa (3.2×10^4 ksi) and 2.16×10^5 MPa (3.1×10^4 ksi) for thicknesses of 0.42 mm (0.017 in.) and 0.60 mm (0.024 in.) respectively. The three values for two thicknesses were based on different batches of sheets used in the study. Care was taken to match the coupons with the particular test specimens. Further details are given in Yang and Hancock (2002).

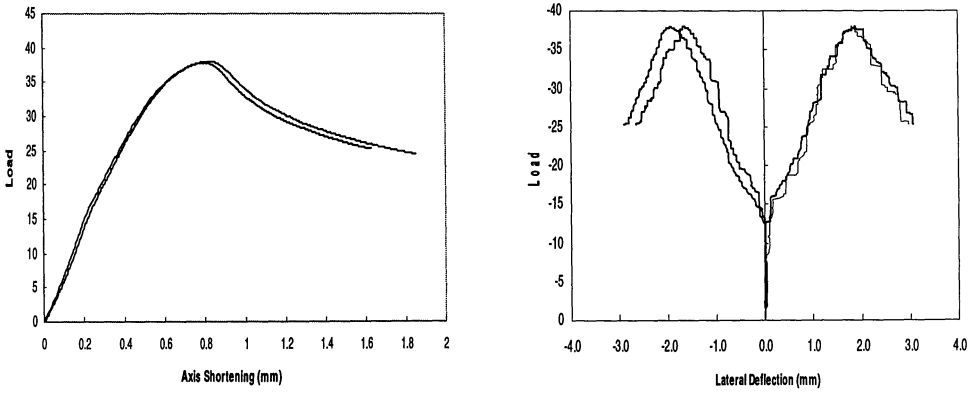

Fig.4 Typical Load-shortening & Local-deflection curves of stub column

STUB COLUMN TESTS

Testing

The rig consisted of the Sintech/MTS-300kN (67 kips) testing machine with fix-ended bearings. The bottom bearing was adjustable so that it could orient specimens vertically. However, Pattenstone was needed at the top to ensure perfect contact. The load and shortening were recorded using the Sintech data acquisition system. The compressive deformation rate was 0.05 mm/min (0.002 in./min).

The central deflections were measured using six transducers for the HB-sections. For the LB-sections, four transducers and two transducers were used for the sides and the lips respectively. For the B-sections, four transducers were used, two for the plate and two for the lips. The transducers were connected to a SPECTRA data acquisition system.

Test specimen behaviour, ultimate load-capacity and experimental local buckling loads

As shown in Fig. 4, initially the columns remained elastic with the slope associated with axial stiffness approximately constant. Stiffening occurred at take-up initially in some specimens. At local buckling, as demonstrated by the lateral deflections, the axial stiffness reduced with the following stiffness getting smaller and smaller until the ultimate load was reached. After that point the load decreased but the unloading stiffness did not fall too sharply.

From observation of the surface of the specimen, the buckling behaviour can be seen. After the first lateral deflections occurred, elastic local buckling can be observed with three half-wavelengths occurring along the specimen length. Eventually the column entered the elastic-plastic state and the ultimate load was reached when the local plastic mechanism formed.

From observation of the surface of the specimen, the buckling behaviour can be seen. After the first lateral deflections occurred, elastic local buckling can be observed with three half-wavelengths occurring along the specimen length. Eventually the column entered the elastic-plastic state and the ultimate load was reached when the local plastic mechanism formed. The box-specimens with low b/t ratios (from 33.3 to 66.6) developed roof-shaped mechanisms and those with high b/t ratios developed the so-called flip-disc mechanisms with alternating concavity and convexity at the four sides. The plots of load-deflection also show that the lips did not stay straight during the tests. For some specimens, the deflection of the lips occurred before the elastic buckling load was reached.

The ultimate loads (P_t) for all specimens are given in Figs. 5 & 6 and Appendix 1. The results in Figs. 5 & 6 have been non-dimensionalised with respect to the theoretical stub column strength (N_s) computed to AS/NZS 4600 based on the measured data, as discussed latter. A significant change occurs at b/t equal to about 50 (i.e. b=30 mm (1.18 in.) for t=0.60 mm (0.024 in.) or b=21 mm (0.83 in.) for t=0.42 mm (0.017 in.)), which is equivalent to a minimum value of the non-dimensional strength between 0.85 and 0.9.

The experimental local buckling loads (P_{cr}) were evaluated from the plots of load-deflection and load-shortening. For the plots of load-deflection, the P-w^2 method (Ventaramaiah and Roorda, 1982) was used to obtain the experimental elastic local buckling load. The experimental local buckling loads (P_{cr}) are given in Appendix-1 and Yang and Hancock (2002). As the width of cross-section (b) of column became larger, the experimental elastic local buckling loads (P_{cr}) became smaller with the ultimate load (P_t) increasing. The ultimate load (P_t) was about 5 times the elastic buckling load (P_{cr}) for the largest sections.

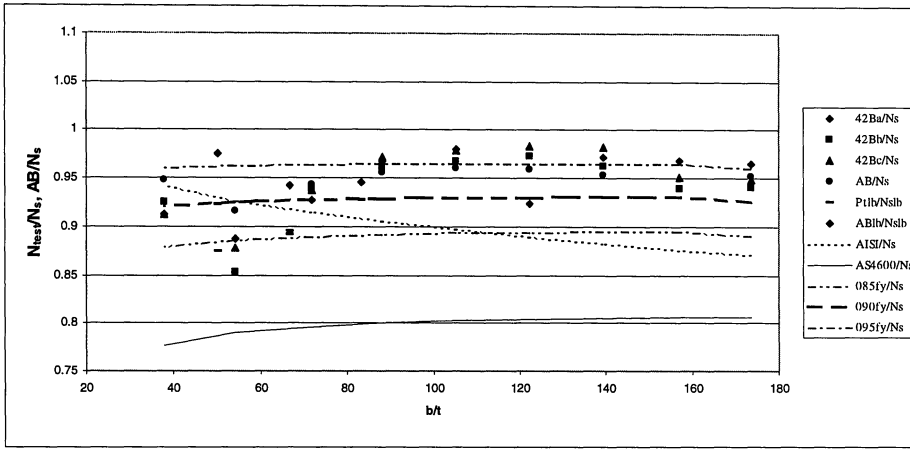

Fig.5 Comparison of B&LB-section Test Results with Design Standard (0.42 mm)

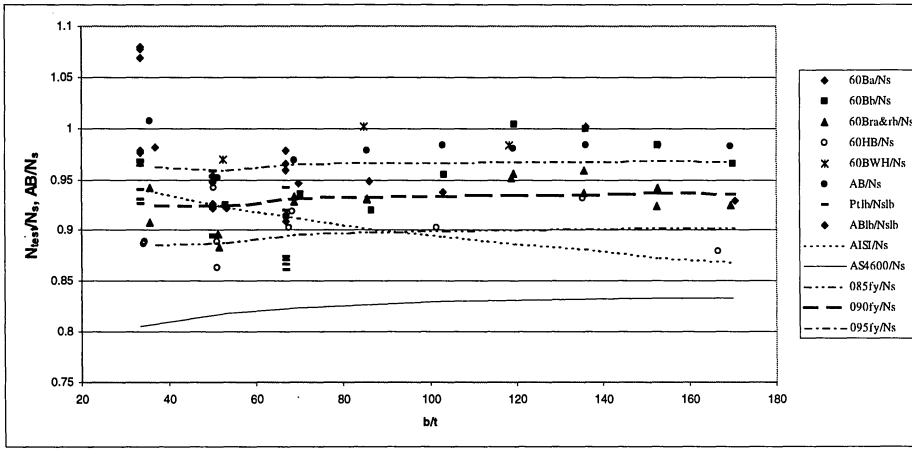

Fig.6 Comparison of B&LB&HB-section Test Results with Design Standard (0.60mm)

ANALYSES

Elastic local buckling analyses

The theoretical elastic local buckling loads (N_{ol}) were obtained using the THIN-WALL program (Papangelis and Hancock, 1998). The average measured cross-section dimensions of the specimens for each series as well as the measured values of base metal thickness and Young's modulus taken from the coupon tests were used to determine the theoretical local buckling loads.

The theoretical local buckling stresses (f_{ol}) varied from approximately 30 MPa (4.4 ksi) for the largest B-sections to 710 MPa (103 ksi) for the smallest B-sections. The effect of the double thickness corner (lip) elements was to increase the theoretical local buckling coefficient (k) for the flat elements from the simply supported value of 4.0 to approximately 4.5 due to slight torsional restraint at each of two corners. The local buckling stresses (f_{ol}) varied from 220 MPa (32 ksi) for the large LB-sections to 960 MPa (139 ksi) for the small LB-sections in 0.60 mm (0.024 in.) thickness. For the LB sections in 0.42 mm (0.017 in.) thickness, three sections were fabricated (30, 40 and 50 mm) (1.18, 1.57 and 1.97 in.) with the same length of lip (5.25 mm) (0.21 in.). The local buckling stresses ranged from 70 MPa (10 ksi) to 185 MPa (27 ksi) for LB-sections in 0.42 mm (0.017 in.) thickness. The effect of the two webs with the double thickness lips was to increase the theoretical local buckling coefficient (k) for the flanges to approximately 5.6. This value is between the values for the simply supported edges (k=4) and the built-in edges (k=6.97). (Bulson, 1970). The lips attached to the web elements can be regarded as an intermediate stiffener similar to those discussed by Desmond, Pekoz and Winter (1981). However, they are of sufficient size to ensure that the web elements buckle in an anti-symmetric mode with the stiffener preventing movement normal to the plane of the web elements. The local buckling stresses (f_{ol}) varied from 32 MPa (4.6 ksi) for the large HB-sections to 760 MPa (110 ksi) for the small HB-sections in 0.60 mm (0.024 in.) thickness. The hexagonal sections were assumed to have a buckling coefficient of 4.0 for all faces. The theoretical local buckling coefficient (k) for all faces is about 4.5 due to slight restraint at the Teflon supports. It was similar to the B-sections. Some restraint at the supports is visible. The theoretical local buckling mode is shown in Yang and Hancock (2002).

The full set of ratios of the experimental local buckling loads (P_{cr}) to the theoretical local buckling load (N_{ol}) are given in Yang and Hancock (2002). The mean ratios are 0.90 with a buckling coefficient average value of 4.8. These results indicate that the THIN-WALL program was in reasonably good agreement with the experimental local buckling loads.

Finite Element Non-linear Analyses

The finite element non-linear analysis program "ABAQUS" was used to simulate the behaviour of columns. The ratios of the ABAQUS simulations (AB) to the theoretical stub column

strengths are also shown in Figs. 5 & 6. Further details are given in Yang and Hancock (2002), such as element type, material behaviour, boundary conditions and geometrical imperfection.

For the stockiest B-sections, the ABAQUS results were very sensitive to the imperfections as shown in Fig. 6 for the 30 mm (1.18 in.) sections. In order to clarify the degree of imperfection sensitivity, a further investigation was performed. Two steps were involved in setting up the analyses. The first step was an eigenvalue buckling analysis performed on the "perfect" column to establish buckling modes. The second step was creating an imperfection in the geometry by adding these modes to the "perfect" geometry. The lowest buckling modes are assumed to provide the most critical imperfections, so usually these are scaled and added to the perfect geometry to create the perturbed mesh. The magnitudes of the perturbations used are a percentage of the sheet thickness.

The degree of initial imperfection was specified as the maximum amplitude of the buckling mode shape and was usually prescribed as a percentage of the thickness of sheet steel. Walker's (Walker, 1975) suggested expression for the degree of imperfection is $0.3(P_y/P_{cr})^{1/2}t$, where P_y is the yield load and P_{cr} is the critical buckling load, and t is the thickness of sheet steel. Comparing the imperfection values measured with the results based on Walker's suggested expression, the difference was very small. So the results based on the Walker's suggested expression were used in the finite element analyses.

As shown in Figs. 5 & 6, the differences between the results of ABAQUS and tests for the stockiest sections were larger compared with those of the other sizes. It can be seen that the yield stress of the material (f_y) and the local buckling stress (f_{ol}) were about equal for these sections. The analysis of equilibrium indicates that the bifurcation of equilibrium will occur when the critical load is reached. It means that when the yield stress is about equal to the critical buckling stress, the structure will be very sensitive to initial imperfection. Although the values adopted in ABAQUS were based on the measurements and Walker's suggested expression, the differences between the results of ABAQUS and the tests were still quite large for the stocky sections. The main reason for the differences may be very difficult to determine accurately due to the difficulty in determining the true initial imperfection in the sections. For the stockiest B-sections in 0.42 mm (0.017 in.) thickness, the input scale factor varied from 0.05, 0.2 to 0.5. The differences in the computed strengths were approximately 10% and 20% respectively. For the stockiest B-section in 0.60 mm (0.024 in.) thickness, the differences were approximately 3% corresponding to the input scale factor 0.05 and 0.5. For other sections in both thicknesses, the differences were less than 1%. So for the stockiest B-section, the thinner the sheet used, the more sensitive they became to the imperfection.

Comparisons with design standards & ABAQUS

The theoretical stub column strengths (N_s) were calculated according to AS/NZS 4600 (1996). The theoretical strengths were calculated using the average measured cross-section dimensions and the measured material yield stress. The test results (P_t) and ABAQUS (AB) results non-dimensionalised with respect to the theoretical stub column strength (N_s) are plotted against the

plate slenderness ratios (b/t) in Figs. 5 & 6. Solid and dotted curves are also plotted in Figs. 5 & 6. The dotted curve is the ratio of N_{sRb}/N_s versus plate slenderness (b/t). N_{sRb} has been calculated based on $R_b f_y$ as included in Section A3.3.2 of AISI Specification Supplement No.1 (1999). The solid curve is the ratio of $N_{s0.75}/N_s$ versus the plate slenderness (b/t). $N_{s0.75}$ has been calculated based on $0.75f_y$ as included in Clause 1.5.1.5(b) of AS/NZS 4600:1996.

The holes in the lips of the sections were taken into account in the calculation of the theoretical stub column strength (N_s) by simply removing the area from the lips. The plate slenderness (λ) for the lips was less than 0.673 when the width of lip was less than 8.7 mm (0.34 in.) according to Eq. 2.2.1.2(4) of AS/NZS 4600. Hence the lips were fully effective for all B-sections and most LB-sections. For the sections with holes in the lips, the perforated part was treated as an ineffective portion. So the effective width of the lip was the full length of the lip with the diameter of the hole removed. This effective width was used in the calculation of the theoretical stub column strength (N_s). For the others without holes in the lips, the calculation of the theoretical stub column strength (N_s) was based on Clause 2.2.1.2 of AS/NZS 4600:1996 (B2.1 of the AISI Specifications) with an appropriate slenderness (λ). The plate buckling coefficient (k) values were as specified in Clause 2.2.1.2 of AS/NZS 4600 (B3.1 of the AISI Specifications) for stiffened sections and Clause 2.3.1 of AS/NZS 4600 (B2.1 of the AISI Specifications) for the unstiffened sections.

In this paper, the plots were based on the P_t/N_s ratio vs. b/t ratio rather than the f_{max}/f_y ratio vs. b/t ratio which was used by Wu, Yu and Laboube (1996). The reason may be explained as follows. In their tests, the ultimate stress f_{max} was obtained from the measured average compressive edge strain and the average tensile strain was recorded at the failure of each panel. The problem with this method may be that the change of the strain or stress on the surface of the specimens can be very large from point to point to produce scatter in the data so that it may have been difficult to obtain an accurate curve with this method.

The ratios P_t to N_s of for the B-sections in 0.42 mm (0.017 in.) and 0.60 mm (0.024 in.) thickness plotted against the plate slenderness (b/t) are shown in Figs. 5 & 6 identified using symbols (♦, ■, ▲). It can be seen that both thicknesses had a similar tendency. The ratios of P_t/ N_s decreased when the plate slenderness (b/t) varies from 33 to 50. In this range, the test results are close to the results based on the AISI Specification Supplement No.1 (1999) and also have the same tendency. As the plate slenderness (b/t) varies from 50 to 116, the ratios (P_t/ N_s) increase. However, for plate slenderness (b/t) greater than 116, the ratios (P_t/ N_s) decrease slightly. It can be noted that for the B-section in 0.60 mm (0.024 in.) thickness the test results show more scatter than those of the B-section in 0.42 mm (0.017 in.) thickness. The "♦" and "■" points are for the B-sections in 0.60 mm (0.024 in.) thickness with holes in the lips at 20 mm (0.79 in.) spacing, whereas the "▲" points are for the B-sections in 0.60 mm (0.024 in.) thickness with holes in the lips at 10 mm (0.39 in.) spacing. It is obvious that the latter are lower than the former by about 5%. To clarify the effect of the holes on the column strength, three different sizes (30,50 and 70 mm plate width) (1.2, 2.0, and 2.8 in.) of B-sections in 0.60 mm (0.024 in.) thickness were fabricated and tested with clamps on the lips. The test results (BWH) are shown in Fig. 6 expressed by the "*" points. It can be seen that the results obtained by simply removing the holes from the net area when calculating N_s may underestimate the column strengths by about 5%.

The ratios of the ABAQUS strengths (AB to N_s) for the B-sections in 0.42 mm (0.017 in.) and 0.60 mm (0.024 in.) plotted against the plate slenderness (b/t) are also shown in Figs. 5 & 6 expressed using symbols (●). For the B-sections in 0.42 mm (0.017 in.) thickness, the ABAQUS results are in good agreement with the test results. However, for the B-sections in 0.60 mm (0.024 in.) thickness, the ABAQUS results were about 5% higher than the test results obtained from sections with holes in their lips and slightly lower than the test results obtained for sections without holes. The ABAQUS analysis did not model the holes but the area of the holes was deducted.

Only three different sizes were tested for the LB-sections in 0.42 mm (0.017 in.) and 0.60 mm (0.024 in.) thickness respectively. The ratios of P_t to N_s for the LB-sections in 0.42 mm (0.017 in.) and 0.60 mm (0.024 in.) thickness plotted against the plate slenderness (b/t) are shown in Figs. 5 & 6 identified using symbols (—). It can be seen that for the LB-sections in 0.42 mm (0.017 in.) thickness, the tendency is quite similar to that of the B-sections but a little bit lower by about 2% for the smaller and bigger sizes and 5% for the medium size compared with values at the equivalent plate slenderness (b/t) of the B-sections. The tendency is contrary to the curve based on AISI Specification Supplement No.1(1999). The largest difference of 5% occurs for the largest size column. For the LB-sections in 0.60 mm (0.024 in.) thickness, it can be seen that the test results are more scattered, however the tendency of the average value is still similar to that of the B-sections.

The ratios of the ABAQUS strengths (AB to N_s) for the LB-sections in 0.42 mm (0.017 in.) and 0.60 mm (0.024 in.) plotted against the plate slenderness (b/t) are shown in Figs. 5 & 6 expressed using symbols (◊). The ABAQUS results for the LB-sections in 0.42 mm (0.017 in.) thickness are a little bit higher than the test results by about 2% and 5% for the big and small sizes respectively. For the LB-sections in 0.60 mm (0.024 in.) thickness, the ABAQUS results were close to the test results except for some of the results of the small sizes for which ABAQUS was somewhat higher as discussed earlier.

HB-sections were tested in the 0.60 mm (0.024 in.) thickness only. The ratios of the test results (P_t) to the theoretical stub column strengths (N_s) of the HB-sections in 0.60 mm (0.024 in.) thickness plotted against the plate slenderness (b/t) are shown in Fig. 6 identified using symbols (○). The results show a similar trend to the B&LB sections but are lower at high slenderness with the last test value quite low. It appears that the Teflon may not have fully restrained the sheet at high slenderness. The ratio of the ABAQUS strengths (AB to N_s) of the HB-sections 0.60 mm (0.024 in.) plotted against the plate slenderness (b/t) are also shown in Fig. 6 identified using the symbols (♦). As can be seen, the larger the section, the higher the ultimate load became except for the largest section. For the last three sections, the differences of results between ABAQUS and tests were 5%, 5% and 12% respectively. The high slenderness test results seem to be faulty as discussed above.

MODIFIED REDUCTION FACTOR

In Figs. 5 & 6, it can be seen that the ratios of the test results and theoretical values became higher as the sections became slender. The tendency of the test results was contrary to the results based on the AISI Specification Supplement No.1 (1999). Although the test results and the results based on AS/NZS 4600 using a 75% reduction in the yield stress have the same tendency, those predicted results are too conservative to utilize fully the strength of material.

From the test data, it appears that a modified reduction factor should be used. Three trial reduction factors (0.85, 0.90 and 0.95) were chosen to be used to calculate the section capacity. The results ($N_{s0.85}$, $N_{s0.90}$ and $N_{s0.95}$) based on those reduction factors were obtained respectively. The dash double-dot, dash and dash-dot curves are plotted in Figs. 5 & 6, which are the ratios of $N_{s0.85}/N_s$, $N_{s0.90}/N_s$ and $N_{s0.95}/N_s$ versus the plate slenderness (b/t).
As can be seen in Figs. 5 & 6, the dash curves based on the reduction factor of 0.90 fits the mean tests well. So the modified reduction factor 0.90 can be used to replace the reduction factor 0.75, which is specified for G550 steel with the thickness being less than 0.9 mm (0.035 in.) in AS/NZS 4600.

CONCLUSIONS

A range of stub columns in G550 sheet steel to AS1397 has been tested in compression to obtain the strength characteristics of this steel with low strain-hardening. The following detailed observations & conclusions can be made.

- As detailed in Yang and Hancock (2002), for the stockiest sections, the average ultimate stress (P_t/A) was lower than the theoretical local buckling stress (f_{ol}) due to the effect of yielding and initial imperfections. However for the slender sections, the average ultimate stress (P_t/A) was higher than their local buckling stress (for the biggest sections, about 5 times the local buckling stress) as a result of the post-buckling effect even though the initial imperfection was bigger than that of the stockiest sections. As shown in Figs. 5 & 6, the maximum non-dimensional section strength is reached when the plate slenderness (b/t) is equal to 120.

- The effect of holes on the ultimate load should be considered. Many researchers have investigated perforated members under compression. Levy, Woolley and Kroll (1947) studied circular holes in the simply supported square plate, and found that if the diameter of a hole is half of the width of the plate, the buckling load will drop by 14%. In the tests in this report, sections with holes in the lips, for which the diameter of the holes was nearly 50% of the width of the lips, had an effect on the ultimate load which made it decrease by about 13%. However, a significant effect on the buckling load was not observed. So for the sections with holes in the lips, the ultimate loads may be considered to be about 87% of those of the same section without holes in the lips if the diameter of hole is near 50% of the lip width.

- Walker's (Walker, 1975) suggested expression used to scale initial imperfections in an ABAQUS model was generally successful. Based on P_y and P_{cr} of such thin sheet steel sections, this expression can provide an initial imperfection magnitude suitable for the simulation of the test results.

- The use of the finite element program ABAQUS for simulating the behaviour of the stub columns was successful since the ABAQUS results were generally in good agreement with experimental values. The results of ABAQUS were sensitive to the initial imperfections for the stockier sections but not for the slender sections. ABAQUS can be used for further work on such thin sheet steel sections.

- The results of the successful stub column tests have been compared with the design procedures in the Australian/New Zealand Standard for Cold-formed Steel Structures and recent (1999) Amendments to the American Iron and Steel Institute Specification. As expected, the greatest effect of the low strain hardening was for the stockier sections where material properties play an important role. For the more slender sections where elastic local buckling and post-local buckling are more important, the effect of low strain hardening does not appear to be as significant. This is contrary to recent design proposals in the USA (Wu, Yu and LaBoube) where it was believed that the more slender sections had been influenced. This design proposal was based on the plots of the f_{max}/f_y ratio vs. b/t ratio of Deck Panel Tests.

- As shown in Fig. 5 & 6, the ratios of AB/N_s and P_t/N_s were mostly larger than 0.90 and higher than the results based on the AISI Specification Supplement No.1 (1999) and AS/NZS 4600 when the plate slenderness (b/t) was greater than 88. When the plate slenderness (b/t) was less than 50, the formulae used in AISI Specification Supplement No.1(1999) was slightly unconservative due to the imperfection sensitivity. The conclusion drawn from the test results is that for stub compression members, $0.90f_y$ may be used as the reduced yield point to determine the nominal strength of the stub columns.

ACKNOWLEDGEMENTS

This paper forms a part of an ARC research project entitled "Compression Stability of High Strength Steel Sections with Low Strain-Hardening" being carried out in the Department of Civil Engineering at the University of Sydney. The authors would like to thank the Australian Research Council and BHP Coated Steel Australian for their financial support for these projects performed at the University of Sydney. The tensile specimens were milled in the Willam and Agnes Bennet Supersonics Laboratory in the Department of Aeronautical Engineering. The compression specimens were fabricated in the J.W. Roderick Laboratory for Materials and Structures in the Department of Civil Engineering. The authors would like to thank Mr. Todd Budrodeen for fabricating the specimens and designing the rig for imperfection measurement. The advice of Associate Professor Kim Rasmussen on the compression tests is gratefully acknowledged. The first author is supported by a joint Department of Civil Engineering and Centre for Advanced Structural Engineering Scholarship.

REFERENCES

Abdel-Sayed, G., "Effective width of thin plates in compression", Journal of Structural Engineering, Vol.95, No.10, Oct. 1969.

Alexander W., "Columns and struts", E. & F. Spon, Ltd., New York, 1912.

American Iron and Steel Institute. (1997). "1996 Edition of the Specification for the Design of Cold-Formed Steel Structural Members", Washington, DC, USA.

American Iron and Steel Institute. (2000). "1996 Edition of the Specification for the Design of Cold-Formed Steel Structural Members, Supplement 1, July 1999", Washington, DC, USA.

American Society for Testing and Materials A611. (1997). "Standard Specification for Steel Sheet, Carbon, Cold-Rolled, Structural Quality", Philadelphia, PA, USA

American Society for Testing and Materials A653. (1997). "Standard Specification for Steel Sheet, Zinc-Coated (Galvanized) or Zinc-Iron Alloy-Coated (Galvannealed) by the Hot-Dip Process", Philadelphia, PA, USA.

American Society for Testing and Materials A792. (1994). "Standard Specification for Steel Sheet, 55% Aluminum-Zinc Ally-Coated by the Hot-Dip Process", Philadelphia, PA, USA

Bulson P.S., "The stability of flat plates", Chatto & Windus Ltd, 1970.

Desmond T.P, Pekoz T, and Winter G., "Intermediate stiffeners for thin-walled members", Journal of Structural Engineering, Vol.107, No.4, April 1981.

Hibbitt, Karlsson & Sorensen, Inc., "ABAQUS/Standard User's Manual", Ver.5.7, 1997

Levy, S. Wooley, R.M., and Kroll, W.D., "Instability of simply supported square plate with reinforced circular hole in edge compression", Research Paper RP1849, Vol.39, Dec. 1947

Mathcad 2000 Professional, (1999), ©1989-1999 Mathsoft Inc..

McAdam, J.N, Brockenbrough, R.A., LaBoube, R.A., Pekoz, T, and Schneider, E.J., "Low strain hardening ductile steel cold-formed members", 9th International Specialty Conference on Cold-Formed Steel Structures, St Louis, Missouri, Nov 1988.

Miller T.H., Pekoz T., "Unstiffened strip approach for perforated wall studs", Journal of Structural Engineering, Vol.120, No.2, Feb., 1994

Papangelis, J.P., Hancock, G.J. THIN-WALL 2.0 (1998), Centre for Advanced Structural Engineering, Department of Civil Engineering, University of Sydney.

Rogers, C.A., Hancock, G.J. (1997). "Ductility of G550 sheet steels in tension", Journal of Structural Engineering, ASCE, Vol. 123, No. 12, 1586-1594.

Rogers, CA, Yang, D. and Hancock, GJ, "Stability and ductility of thin high-strength G550 steel sections and connections", Proceedings, International Conference on Thin-Walled Structures, Poland June, 2001

Roger, C.A., Hancock, G.J., "Ductility of G550 sheet steels in tension-elongation measurements and perforated tests", Research Report No. R735, School of Civil and Mining Engineering, University of Sydney, 1996.

Standards Australia / Standards New Zealand. (1996). "Cold-formed steel structures - AS/NZS 4600", Sydney, NSW, Australia

Standards Australia. (1991). "Methods for tensile testing of metals-AS 1391-1991", Sydney, NSW, Australia

Standards Australia. (1993). "Steel sheet and strip - Hot-dipped zinc-coated or aluminum/zinc coated - AS 1397", Sydney, NSW, Australia

Venkataramaiah, K.R., Roorda, J., "Analysis of local plate buckling experimental data", 6th International Specialty Conference. on Cold-Formed Steel Structures, St. Louis, Missouri, 1982.

Walker, A. C., "Design and analysis of cold-formed sections", International Textbook Company Limited, 1975

Wu, S., Yu, W.W, and LaBoube, R.A. (1996a), "Strength of flexural members using structural Grade 80 of A653 steel (deck panel tests)", Second Progress Report, Department of Civil Engineering, University of Missouri-Rolla, November.

Wu, S., Yu, W.W, and LaBoube, R.A. (1996b), "Flexural members using structural Grade 80 of A653 Steel (deck panel tests)", 13th International Specialty Conference on Cold-Formed Steel Structures, St Louis, Missouri, 1996.

Yang, D., Hancock, G.J., "Compression tests of cold-reduced high strength steel stub column", Research Report No. R815, School of Civil and Mining Engineering, University of Sydney, 2002.

NOTATION

A	cross-sectional area
AB	ultimate load of ABAQUS
A_e	effective of area
A_{eq}	equivalent effective of area
b	web/flange width
d	lip width
E	Young's modulus of elasticity
f_{ol}	elastic buckling stress
f_y	yield stress
h	flange width
hl	glued lips thickness
L	length of column
N_{ol}	elastic buckling load
N_s	nominal section compression capacity based on f_y
$N_{s0.75}$	nominal section compression capacity based on 0.75 f_y
N_{sRb}	nominal section compression capacity based on $R_b f_y$
P_{cr}	elastic buckling test load
P_t	ultimate test load
P_y	squash load
r	radius of corner
R	radius of corner
t	thickness
t_b	thickness of base metal
t_c	thickness of coated metal

APDENDIX-1

Table 1a. Measured Dimensions of Box Shaped (B) Sections (0.60 mm) & Test Loads

Specimen	Web	Thickness		Radius		Lip	Thickness of lip	Length	Ultimate test load	Elastic buckling test load
	b (mm)	t_h (mm)	t_c (mm)	r (mm)	R (mm)	d (mm)	hl (mm)	L (mm)	P_t (kN)	P_{cr} (kN)
060B20a	22.1	0.60	0.65	0.60	1.20	7.2	1.6	59.7	35.20	N/A
060B20b	22.0	0.60	0.65	0.60	1.20	7.3	1.6	58.5	30.40	N/A
060B30a	31.8	0.60	0.65	0.60	1.20	7.4	1.4	89.5	35.80	29.90
060B30b	31.8	0.60	0.65	0.60	1.20	7.3	1.4	90.2	35.70	31.31
060B40a	41.8	0.60	0.65	0.60	1.20	7.5	1.6	119.3	38.10	22.9
060B40b	42.1	0.60	0.65	0.60	1.20	7.6	1.6	119.6	37.80	22.38
060B50a	51.7	0.60	0.65	0.60	1.20	7.6	1.7	149.9	39.10	17.29
060B50b	51.9	0.60	0.65	0.60	1.20	7.6	1.7	150.0	37.80	17.01
060B60a	61.9	0.60	0.65	0.60	1.20	7.5	1.7	178.9	39.00	13.39
060B60b	61.9	0.60	0.65	0.60	1.20	7.4	1.6	180.2	39.40	13.66
060B70a	71.8	0.60	0.65	0.60	1.20	7.4	1.6	210.0	N/A	N/A
060B70b	71.7	0.60	0.65	0.60	1.20.	7.4	1.6	209.3	41.80	10.64
060B80a	81.8	0.60	0.65	0.60	1.20	7.4	1.5	239.9	42.00	11.05
060B80b	81.7	0.60	0.65	0.60	1.20	7.4	1.6	240.4	42.00	9.53
060B90a	91.7	0.60	0.65	0.60	1.20	7.5	1.9	270.0	N/A	N/A
060B90b	91.6	0.60	0.65	0.60	1.20	7.4	2.0	269.7	41.50	10.28
060B100a	102.3	0.60	0.65	0.60	1.20	7.3	1.7	298.2	39.20	8.57
060B100b	102.1	0.60	0.65	0.60	1.20	7.5	1.7	295.4	41.10	8.44

Note: 1in.=25.4 mm; 1kip=4.448 kN; All specimens with holes at 20 mm spacing

Table 1b. Measured Dimensions of Box Shaped (B) Sections (0.60 mm) & Test Loads

Specimen	Web	Thickness		Radius		Lip	Thickness of Lip	Length	Ultimate test load	Elastic buckling test load
	b (mm)	t_h (mm)	t_c (mm)	r (mm)	R (mm)	d (mm)	hl (mm)	L (mm)	P_t (kN)	P_{cr} (kN)
060B20ra	21.3	0.60	0.65	0.60	1.20	7.5	1.5	59.2	33.89	N/A
060B20rb	21.3	0.60	0.65	0.60	1.20	7.4	1.5	58.9	32.59	N/A
060B30ra	30.7	0.60	0.65	0.60	1.20	7.5	1.6	88.6	34.67	32.94
060B30rb	30.8	0.60	0.65	0.60	1.20	7.5	1.6	88.8	34.13	32.81
060B40ra	41.3	0.60	0.65	0.60	1.20	7.3	1.8	119.0	37.14	23.60
060B40rb	41.2	0.60	0.65	0.60	1.20	7.4	1.8	118.3	37.11	23.75
060B50ra	51.3	0.60	0.65	0.60	1.20	7.5	1.5	148.6	38.13	16.25
060B50rb	51.3	0.60	0.65	0.60	1.20	7.4	1.6	148.9	37.94	15.63
060B60ra	N/A	N/A	N/A	N/A	N/A	N/A	N/A	N/A	N/A	N/A
060B60rb	N/A	N/A	N/A	N/A	N/A	N/A	N/A	N/A	N/A	N/A
060B70ra	71.6	0.60	0.65	0.60	1.20	7.1	1.7	209.0	39.44	11.88
060B70rb	71.4	0.60	0.65	0.60	1.20	7.1	1.7	209.1	39.20	10.63
060B80ra	82.0	0.60	0.65	0.60	1.20	7.6	1.4	240.0	40.61	10.03
060B80rb	82.0	0.60	0.65	0.60	1.20	7.9	1.4	238.7	38.63	9.55
060B90ra	91.7	0.60	0.65	0.60	1.20	7.2	1.7	268.5	39.45	10.52
060B90rb	91.5	0.60	0.65	0.60	1.20	7.2	1.9	267.0	38.67	8.75
060B100ra	101.4	0.60	0.65	0.60	1.20	7.6	1.7	299.2	36.77	6.70
060B100rb	101.7	0.60	0.65	0.60	1.20	7.5	1.7	299.8	39.30	6.90

Note: 1in.=25.4 mm; 1kip=4.448 kN; All specimens with holes at 10 mm spacing

Table 1c. Measured Dimensions of Box Shaped (B) Sections (0.60 mm) & Test Loads

Specimen	Web	Thickness		Radius		Lip	Thickness of Lip	Length	Ultimate test load	Elastic buckling test load
	b (mm)	t_h (mm)	t_c (mm)	r (mm)	R (mm)	d (mm)	hl (mm)	L (mm)	P_t (kN)	P_{cr} (kN)
BWH30	31.5	0.60	0.65	0.60	1.20	7.2	1.4	90.4	42.1	31.64
BWH50	50.9	0.60	0.65	0.60	1.20	7.3	1.5	150.1	45.7	18.01
BWH70	71.1	0.60	0.65	0.60	1.20	7.1	1.7	210.1	45.5	12.21

Note: 1in.=25.4 mm; 1kip=4.448 kN; All specimens without holes

Table 1d. Measured Dimensions of Lipped-Box Shaped (LB) Sections (0.60 mm) & Test Loads

Specimen	Flange	Web	Thickness		Radius		Lip	Thickness of Lip	Length	Ultimate test load	Elastic buckling test load
	h (mm)	b (mm)	t_h (mm)	t_c (mm)	r (mm)	R (mm)	d (mm)	hl (mm)	L (mm)	P_t (kN)	P_{cr} (kN)
060LB20a	10.4	20.8	0.60	0.65	0.60	0.60	5.9	1.3	59.2	37.00	N/A
060LB20b	10.4	20.9	0.60	0.68	0.60	0.60	5.7	1.3	58.4	38.00	N/A
060LB30a	14.9	32.2	0.60	0.69	0.60	0.60	8.2	1.3	89.7	48.70	35.71
060LB30b	15.0	31.6	0.60	0.65	0.60	0.60	8.0	1.4	89.5	N/A	N/A
060LB40a	19.7	42.4	0.60	0.64	0.60	0.60	10.6	1.6	119.5	53.01	N/A

Note: 1in.=25.4 mm; 1kip=4.448 kN; All specimens without holes

Table 1e. Measured Dimensions of Lipped-Box Shaped (LB) Sections (0.60 mm) & Test Loads

Specimen	Flange	Web	Thickness		Radius		Lip	Thickness of Lip	Length	Ultimate test load	Elastic buckling test load
	h (mm)	b (mm)	t_b (mm)	t_c (mm)	r (mm)	R (mm)	d (mm)	hl (mm)	L (mm)	P_t (kN)	P_{cr} (kN)
060LB20ra	10.7	20.3	0.60	0.65	0.60	0.60	6.7	2.7	60.1	37.28	N/A
060LB20rb	10.7	20.7	0.60	0.65	0.60	0.60	6.7	2.1	60.5	35.64	N/A
060LB30ra	15.5	30.6	0.60	0.65	0.60	0.60	6.8	2.4	90.3	45.99	37.50
060LB30rb	15.6	30.5	0.60	0.65	0.60	0.60	6.9	2.3	89.9	45.75	40.13
060LB40ra	20.5	40.9	0.60	0.65	0.60	0.60	6.9	2.4	120.2	47.34	24.30
060LB40rb	20.6	40.8	0.60	0.65	0.60	0.60	6.6	2.3	120.3	44.58	N/A
060LB40b	20.0	41.7	0.60	0.65	0.60	0.60	10.6	1.5	119.4	53.30	28.95

Note: 1in.=25.4 mm; 1kip=4.448 kN; All specimens with holes at 10 mm spacing

Table 1f. Measured Dimensions of Lipped-Box Shaped (LB) Sections (0.60 mm) & Test Loads

Specimen	Flange	Web	Thickness		Radius		Lip	Thickness of Lip	Length	Ultimate test load	Elastic buckling test load
	h (mm)	b (mm)	t_b (mm)	t_c (mm)	r (mm)	R (mm)	d (mm)	hl (mm)	L (mm)	P_t (kN)	P_{cr} (kN)
060LB20na	10.9	20.8	0.60	0.65	0.60	0.60	5.6	1.6	59.6	36.40	N/A
060LB20nb	10.9	20.7	0.60	0.65	0.60	0.60	5.5	1.5	59.2	35.40	N/A
060LB30na	16.1	30.2	0.60	0.65	0.60	0.60	7.8	1.4	89.7	45.80	37.17
060LB30nb	16.0	30.4	0.60	0.65	0.60	0.60	7.9	1.4	89.7	45.80	36.16
060LB40na	20.9	40.7	0.60	0.65	0.60	0.60	10.4	1.4	119.6	50.60	28.11
060LB40nb	21.0	40.6	0.60	0.65	0.60	0.60	10.3	1.4	119.7	51.30	25.19

Note: 1in.=25.4 mm; 1kip=4.448 kN; All specimens with clamps

Table 1g. Measured Dimensions of Hexagonal Shaped (HB) Sections (0.60 mm) & Test Loads

Specimen	Flange	Web	Thickness		Radius	Length	Ultimate test load	Elastic buckling test load
	b_f (mm)	b (mm)	t_b (mm)	t_c (mm)	r (mm)	L (mm)	P_t (kN)	P_{cr} (kN)
060HB20	19.3	20.5	0.60	0.65	1.10	60.1	37.30	N/A
060HB20ra	19.1	20.6	0.60	0.65	1.10	60.0	37.40	N/A
060HB30a	29.3	30.5	0.60	0.65	1.10	89.5	39.90	34.50
060HB30b	29.1	30.9	0.60	0.65	1.10	90.5	43.60	37.22
060HB30c	29.4	30.6	0.60	0.65	1.10	91.0	41.10	35.42
060HB40a	39.2	41.0	0.60	0.65	1.10	119.8	44.36	27.78
060HB40b	40.4	40.5	0.60	0.65	1.10	120.0	43.60	29.44
060HB60	59.6	61.0	0.60	0.65	1.10	179.8	45.36	18.89
060HB80	79.4	81.2	0.60	0.65	1.10	240.1	47.70	14.86
060HB100	99.5	100.0	0.60	0.65	1.10	300.0	45.50	12.86

Note: 1in.=25.4 mm; 1kip=4.448 kN

Table 2a. Measured Dimensions of Box Shaped (B) Sections (0.42 mm) & Test Loads

Specimen	Web	Thickness		Radius		Lip	Thickness of Lip	Length	Ultimate test load	Elastic buckling test load
	b (mm)	t_b (mm)	t_c (mm)	r (mm)	R (mm)	d (mm)	hl (mm)	L (mm)	P_t (kN)	P_{cr} (kN)
042B14a	15.5	0.41	0.45	0.60	1.20	5.7	0.9	41.5	17.10	N/A
042B14b	15.4	0.41	0.45	0.60	1.20	5.7	1.0	41.7	17.30	N/A
042B14c	15.6	0.41	0.45	0.60	1.20	5.7	0.9	41.8	17.10	N/A
042B21a	22.2	0.41	0.45	0.60	1.20	5.7	0.9	62.5	17.70	13.65
042B21b	22.3	0.41	0.45	0.60	1.20	5.5	1.0	62.3	16.80	14.54
042B21c	22.2	0.41	0.45	0.60	1.20	5.6	0.9	62.5	17.40	12.97
042B28a	29.4	0.41	0.45	0.60	1.20	5.7	1.1	83.5	19.10	8.92
042B28b	29.4	0.41	0.45	0.60	1.20	5.5	0.9	83.4	19.10	10.30
042B28c	29.3	0.41	0.45	0.60	1.20	5.7	1.0	83.6	19.30	10.26
042B35a	36.1	0.41	0.45	0.60	1.20	5.5	1.0	104.6	20.00	7.02
042B35b	36.1	0.41	0.45	0.60	1.20	5.6	1.0	104.1	20.00	8.06
042B35c	36.3	0.41	0.45	0.60	1.20	5.5	1.1	104.3	20.10	7.68
042B42a	43.2	0.41	0.45	0.60	1.20	5.5	1.0	125.5	20.50	6.15
042B42b	43.2	0.41	0.45	0.60	1.20	5.4	1.0	125.0	20.50	5.69
042B42c	43.4	0.41	0.45	0.60	1.20	5.4	1.0	125.6	20.50	7.22
042B49a	50.2	0.41	0.45	0.60	1.20	5.6	1.0	146.0	19.60	5.32
042B49b	50.2	0.41	0.45	0.60	1.20	5.7	1.0	146.5	20.80	6.25
042B49c	50.2	0.41	0.45	0.60	1.20	5.7	1.0	146.2	21.00	6.25
042B56a	57.2	0.41	0.45	0.60	1.20	5.7	0.9	167.2	20.90	4.70
042B56b	57.1	0.41	0.45	0.60	1.20	5.7	1.0	165.6	20.70	5.47
042B56c	57.1	0.41	0.45	0.60	1.20	5.7	1.0	165.1	21.10	4.70
042B63a	64.4	0.41	0.45	0.60	1.20	5.7	1.1	188.5	20.90	3.94
042B63b	64.4	0.41	0.45	0.60	1.20	5.7	1.1	187.8	20.30	3.97
042B63c	64.6	0.41	0.45	0.60	1.20	5.5	1.1	187.5	20.30	3.94
042B70a	71.2	0.41	0.45	0.60	1.20	5.7	1.1	209.3	20.90	3.65
042B70b	71.4	0.41	0.45	0.60	1.20	5.7	1.1	208.5	20.40	3.52
042B70c	71.3	0.41	0.45	0.60	1.20	5.6	0.9	209.2	20.45	3.52

Note: 1in.=25.4 mm; 1kip=4.448 kN; All specimens with clamps

Table 2b. Measured Dimensions of Lipped-Box Shaped (LB) Sections (0.42 mm) & Test Loads

Specimen	Flange	Web	Thickness		Radius		Lip	Thickness of Lip	Length	Ultimate test load	Elastic buckling test load
	h (mm)	b (mm)	t_b (mm)	t_c (mm)	r (mm)	R (mm)	d (mm)	hl (mm)	L (mm)	P_t (kN)	P_{cr} (kN)
042LB30a	15.7	32.6	0.41	0.45	0.60	0.60	6.5	1.0	90.6	24.80	12.58
042LB30b	15.7	32.8	0.41	0.45	0.60	0.60	5.8	1.0	90.4	23.50	11.25
042LB40a	20.6	41.6	0.41	0.45	0.60	0.60	6.1	1.0	119.2	25.10	8.92
042LB40b	20.8	41.9	0.41	0.45	0.60	0.60	6.1	1.0	119.8	25.00	8.46
042LB50a	26.0	51.5	0.41	0.45	0.60	0.60	6.0	1.1	150.4	26.10	6.18
042LB50b	25.9	51.7	0.41	0.45	0.60	0.60	5.9	1.1	150.7	26.10	7.08

Note: 1in.=25.4 mm; 1kip=4.448 kN; All specimens with clamps